Local-density-functional methods in two-dimensionally periodic systems. Hydrogen and beryllium monolayers*

J. W. Mintmire,† J. R. Sabin, and S. B. Trickey
Quantum Theory Project, Departments of Physics and Chemistry, University of Florida, Gainesville, Florida 32611

(Received 18 September 1981; revised manuscript received 22 March 1982)

A new computational approach to calculating the electronic structure of thin films is presented in detail. The local-density-functional formalism in the linear combination of atomic orbitals approximation is used. The self-consistent solution of the resulting secular equations is made tractable through the use of efficient fitting procedures to approximate the charge density and its cube root. Feasibility is demonstrated by calculational results for an atomic hydrogen monolayer and an atomic beryllium monolayer. Comparison of the beryllium results with known experimental data on the beryllium surface and other calculations gives respectable agreement.

I. INTRODUCTION

The study of the electronic properties of solid surfaces is becoming increasingly more important as techniques dependent on surface properties take pivotal roles in modern technology. Experimental interest in surfaces has heightened correspondingly in recent years, with greatly refined data coming about in large measure because of improved vacuum techniques. The theoretical study of the electronic properties of extended systems thus faces the challenge to develop new methods for understanding the behavior of the surfaces of these systems. One theoretical approach explored by several groups[1–3] is to calculate the electronic properties of a thin layer (an infinitely periodic structure in two dimensions and of finite thickness in the direction normal to the plane of periodicity) with linear combination of atomic orbitals (LCAO) methods using the Hartree-Fock-Slater local-density-functional method.

Here we present a new computational approach to calculate the approximate two-dimensional band structure and total energy of such a thin-layer system. A preliminary description of this approach[4] (hereafter referred to as I), has already been presented, with sample results for a simple atomic hydrogen monolayer using only *s*-type Gaussian basis functions.

The thin-layer system used possesses both surfaces and the periodicity in directions parallel to the surface which is characteristic of a cleaved bulk solid. A two-dimensional wave vector, Brillouin zone, etc., therefore exist and can be utilized. By increasing the thickness of the slab the interactions between the surfaces decrease and the properties of the semi-infinite solid may be approached as a limit.

In the LCAO treatment of a local density model such as $X\alpha$ (for a review, see Ref. 5), the most difficult problem is efficient construction of the secular matrix. Most of the computational difficulties arise from the need to evaluate matrix elements involving $\rho^{1/3}(\vec{r})$ (where ρ is the electronic charge density). A method of fitting $\rho^{1/3}$ to a linear combination of two-dimensionally periodic fitting functions in a manner equivalent to the scheme of Dunlap *et al.*[6] for molecular systems is developed here. The formalism derived by Dunlap[6] and Mintmire[7] for treating the charge density in the molecular case cannot be used directly for extended systems due to the long-range nature of the Coulomb interaction, which results in singular integrals in the limit of a two-dimensionally periodic slab. Here we devise a scheme equivalent to the original molecular-density scheme[6] but with proper limiting behavior. Our work is similar to the techniques discussed by Feibelman, Appelbaum, and Hamann[3]; the primary differences arise from the fitting techniques utilized. The results may be extended easily to other local density models.

The methodology is tested on two systems: the atomic hydrogen monolayer and the atomic beryllium monolayer. Both *s*- and *p*-type Gaussian atom-

ic orbitals (AO's) were used. The results for the hydrogen monolayer demonstrate the feasibility of the method and illustrate some of the effects of changes in basis sets and in the number of $\vec{k}$ points considered in the surface Brillouin zone. The atomic beryllium results further demonstrate the feasibility of the method, as well as allowing some comparison with experimentally determined results such as the work function and Auger spectra of the beryllium surface.

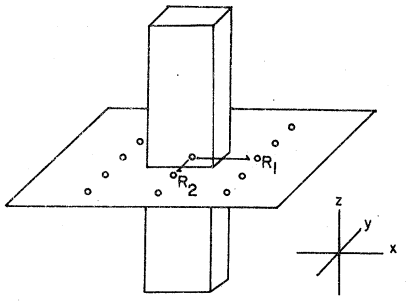

FIG. 1. Illustration of parallelopiped unit cell for the two-dimensionally periodic monolayer. Note that the unit cell extends to infinite distance in both directions parallel to the z axis.

II. MATHEMATICAL FORMALISM

A two-dimensionally infinite periodic system may be defined by the existence of two primitive lattice vectors $\vec{R}_1$ and $\vec{R}_2$, which generate a group of translations $(\vec{R}\,|\,\vec{R}=m\vec{R}_1+\vec{R}_2$, m and n are integers). Any translation by a member of this group yields a point equivalent to the original point. Using these two primitive lattice vectors, we may construct a parallelopiped unit cell as shown in Fig. 1.

We have extended the LCAO-$X\alpha$ method of Dunlap[6] and Mintmire[7] to these two-dimensionally periodic systems. In this approach, the variational principle is used in minimizing the local density functional per unit cell, which has the form (in Hartree atomic units)

$$E[\rho]=-\tfrac{1}{2}\int_\Omega d^3r\sum_{i\,\vec{k}} n_i(\vec{k})\Psi_i^*(\vec{r};\vec{k})\nabla^2\Psi_i(\vec{r};\vec{k})+\int_\Omega d^3r\,\rho(\vec{r})\left[-\sum_a\frac{Z_a}{|\vec{r}-\vec{R}_a|}+\tfrac{1}{2}\int d^3r'\frac{\rho(\vec{r}')}{|\vec{r}-\vec{r}'|}\right]$$
$$+\tfrac{1}{2}\sum_{a\neq b}\frac{Z_aZ_b}{|\vec{R}_a-\vec{R}_b|}+\int_\Omega d^3r\,[\rho\uparrow(\vec{r})V_{ex}\uparrow(\vec{r})+\rho\downarrow(\vec{r})V_{ex}\downarrow(\vec{r})]\,, \tag{1}$$

where $V_{ex}\uparrow$ is Slater's $X\alpha$ exchange potential for spin-up

$$V_{ex}\uparrow(\vec{r})=-\left[\frac{9\alpha}{2}\right]\left[\frac{3\rho_\uparrow(\vec{r})}{4\pi}\right]^{1/3} \tag{2}$$

and the notation Ω indicates an integration over the parallelopiped unit cell.

The one-electron orbitals $\Psi_i(\vec{r};\vec{k})$ are created from a linear combination of Bloch functions $\phi_i(\vec{r};\vec{k})$ such that

$$\Psi_i(\vec{r};\vec{k})=\sum_j C_{ji}(\vec{k})\phi_j(\vec{r};\vec{k})\,, \tag{3}$$

where the Bloch functions are sums of local functions $U_j(\vec{r})$,

$$\phi_j(\vec{r};\vec{k})=\sum_{\vec{R}}\exp(i\vec{k}\cdot\vec{R})U_j(\vec{r}-\vec{R})\,. \tag{4}$$

A discrete set of evenly spaced $\vec{R}$ points is used to describe the two-dimensional Brillouin zone by invoking periodic boundary conditions. Within this framework we construct the one-electron density $\rho(\vec{r})$ as follows:

$$\rho(\vec{r})=\sum_{\vec{k}}\sum_i n_i(\vec{k})\Psi_i^*(\vec{r};\vec{k})\Psi_i(\vec{r};\vec{k})\,. \tag{5}$$

The variational procedure thus yields a secular equation of the form

$$\sum_n H_{mn}(\vec{k})c_{ni}(\vec{k})=E_i\sum_n S_{mn}(\vec{k})c_{ni}(\vec{k})\,, \tag{6}$$

where $S_{mn}(\vec{k})$ is the overlap integral between Bloch functions defined by

$$S_{mn}(\vec{k})=\int_\Omega d^3r\,\phi_m^*(\vec{r};\vec{k})\phi_n(\vec{r};\vec{k})\,. \tag{7}$$

The spin-up effective Hamiltonian matrix elements are defined as

$$H_{mn}(\vec{k})=\int_\Omega d^3r\,\phi_m^*(\vec{r};\vec{k})\left[-\tfrac{1}{2}\nabla^2+\tfrac{1}{2}\int d^3r'\frac{\rho(\vec{r}')}{|\vec{r}-\vec{r}'|}-\sum_{\vec{R}}\sum_m\frac{Z_m}{|\vec{r}-\vec{R}_m-\vec{R}|}-3\alpha\left[\frac{3\rho_\uparrow}{4\pi}\right]^{1/3}\right]\phi_n(\vec{r};\vec{k})\,. \tag{8}$$

The effective Hamiltonian matrix contains a term with an integral proportional to $\rho^{1/3}$; one cannot usually express such integrals in an analytic closed form. One way of alleviating this difficulty for molecular systems is to approximate $\rho^{1/3}(\vec{r})$ by a linear combination of fitting functions $\tilde{G}_m(\vec{r})$, called the exchange fit,

$$\rho^{1/3}(\vec{r}) \simeq \sum_m g_m \tilde{G}_m(\vec{r}) . \tag{9}$$

The exchange fit as a tool for efficient handling of the analytic behavior of $\rho^{1/3}$ was originated by Sambe and Felton[8] with extensions to the analysis and computational method by Dunlap, Connolly, and Sabin[9] and Mintmire.[7] In those previous works the total charge density $\rho(\vec{r})$ was also approximated using a linear combination of a set of charge fitting functions $\tilde{F}_m(\vec{r})$, called the charge fit,

$$\rho(\vec{r}) \simeq \sum_m f_m \tilde{F}_m(\vec{r}) \equiv \tilde{\rho}(\vec{r}) . \tag{10}$$

The charge fit is introduced to reduce the number of primitive integrals which must be computed.

For extended systems the fitting functions $\tilde{G}_m(\vec{r})$ and $\tilde{F}_m(\vec{r})$ are composed of periodic sums of localized functions $G_m(\vec{r})$ and $F_m(\vec{r})$, where a localized function has the property that

$$\lim_{r\to\infty} r^3 G_m(\vec{r}) = 0 . \tag{11}$$

These periodic sums may be expressed in the form

$$\tilde{G}_m(\vec{r}) = \sum_{\vec{R}} G_m(\vec{r}-\vec{R}) , \tag{12}$$

with an exactly analogous relationship for $\tilde{F}_m$ with the F_m's. The exchange fitting coefficients g_m are chosen using a conventional least-squares fitting procedure in which minimization of the weighted sum of the squares of the differences

$$\sum_j w_j \left[\rho^{1/3}(\vec{r}_j) - \sum_m g_m \tilde{G}_m(\vec{r}_j) \right]^2 = 0 \tag{13}$$

yields a matrix equation for the g's which is solved, conventionally, by inversion. The set of weights w_j is chosen to approximate numerical integration values over the unit cell of Fig. 1. This procedure allows a reduction of the total number of numerical integrations required, compared to a process not using fitting procedures, by an approximate factor of N^2/N_x, where N is the number of orbital basis functions and N_x is the number of exchange fitting functions $G_m(\vec{r})$.

Before explaining the procedure for choosing the charge fit coefficients f_m, let us briefly review the methods for approximation charge densities in the molecular case according to the procedures of Refs. 6 and 7. Consider a prototypical molecular charge density $\rho(\vec{r})$ such that ρ decreases more rapidly than r^{-3} in the limit of large r. Then define the electrostatic interaction U of a charge density with itself to be $U = \frac{1}{2}[\rho \mid \rho]$, where

$$[\rho_1 \mid \rho_2] = \int d^3r \int d^3r' \frac{\rho_1(\vec{r})\rho_2(\vec{r}')}{\mid \vec{r}-\vec{r}' \mid} . \tag{14}$$

Let ρ be approximated by another density $\tilde{\rho}$ as defined in Eq. (10). The fitting techniques used in the molecular case minimize the quantity $[\Delta\rho \mid \Delta\rho]$ to yield the equation

$$\sum_n [\tilde{F}_m \mid \tilde{F}_n] f_n = [\tilde{F}_m \mid \rho] , \tag{15}$$

where $\Delta\rho = \rho - \tilde{\rho}$. Note that for the molecular case, the fitting functions $\tilde{F}_m$ are localized and may be taken as equivalent with the functions F_m. The fitting coefficients f_n may then be generated using Eq. (15), again by ordinary inversion.

Applications of these methods to extended systems requires a few modifications. The fitting functions $\tilde{F}_m$ are now formed from the periodic sum of the localized functions $F_m(\vec{r})$ as stated in Eq. (12). The charge interaction expression $[\rho_1 \mid \rho_2]$ must also be modified to avoid dealing with infinite terms. The most convenient definition of this term, if ρ_1 and ρ_2 are periodic extended charge densities, is through the electrostatic interaction *per unit cell*:

$$[\rho_1 \mid \rho_2] = \int_\Omega d^3r \int d^3r' \frac{\rho_1(\vec{r})\rho_2(\vec{r}')}{\mid \vec{r}-\vec{r}' \mid} . \tag{16}$$

Note that Eq. (16) is not identical with Eq. (14), since the present integration is per unit cell. The charge interaction term $[\rho_1 \mid \rho_2]$ is still nonnegative for $\rho_1 = \rho_2$ and ρ_1 having no singularities. In addition, this expression is still invariant with respect to interchange of ρ_1 and ρ_2. This expression for the charge interaction is also convenient because it satisfies two conditions:

(1) For $\tilde{F}_m(\vec{r})$ a periodic function formed from the periodic sum of localized functions $F_m(\vec{r})$ as in Eq. (12), then

$$[\tilde{F}_m \mid \tilde{F}_n] = \sum_{\vec{R}} \int d^3r \int d^3r' \frac{F_m(\vec{r})F_n(\vec{r}'-\vec{R})}{\mid \vec{r}-\vec{r}' \mid} , \tag{17}$$

which is analytically integrable in closed form for

$F_m(\vec{r})$ of Gaussian-type functions;

(2) $[\rho_1 \mid \rho_2]$ is finite if and only if one or both of the charge distributions ρ_1 and ρ_2 satisfy the charge neutrality condition

$$\int_\Omega d^3r\,\rho(\vec{r})=0\ . \tag{18}$$

The first condition is evident upon inspection. The second condition follows from consideration of a limiting procedure which begins with a finite assembly of identical unit cells. The initial assembly is constructed with no embedded voids. The limiting process then consists of arbitrary enlargement of the finite assembly, with the infinitely periodic (in two dimensions) slab the ultimate result. Any such finite assembly has a periodic charge density which satisfies the explicit constraint on asymptotic behavior required by the definition of the molecular charge-density interaction $[\rho_1 \mid \rho_2]$ of Eq. (14). It then follows from Eq. (14) that the charge density belonging to a *single* unit cell is

$$[\rho_1 \mid \rho_2]=\sum_{\vec{R}}{}' \int_\Omega d^3r \int_\Omega d^3r' \frac{\rho_1(\vec{r})\rho_2(\vec{r}')}{\mid \vec{r}-\vec{r}'+\vec{R} \mid}\ , \tag{19}$$

where the primed summation indicates a finite number of terms. In order to carry through a physically reasonable limiting process the single unit cell is conceived as being the most nearly central unit cell of the finite assembly. Similarly the origin of coordinates is associated, for convenience, with the central unit cell. Then for each term of Eq. (19), save for the one corresponding to $\vec{R}=\vec{0}$, the contribution may be expressed *exactly* as a multipole expansion. The behavior of the multipoles is such that the second condition is satisfied (see Ref. 10 for details).

Thus the second condition leads immediately to the observation that Eq. (15) as derived is not usable in a direct manner, since the density involved is purely electronic and manifestly not neutral. For any finite system Eq. (15) may be rewritten as

$$\left[\tilde{F}_m \left| \rho-\sum_n f_n\tilde{F}_n \right.\right]=0\ , \tag{20}$$

irrespective of charge neutrality. In the limit described above, however, the charge interaction expression becomes that of Eq. (16), and the necessary and sufficient conditions on charge neutrality come into play with the result that if at least one of the $\tilde{F}_m$'s is not charge neutral, then the right-hand factor in Eq. (20) must be charge neutral, which implies

$$\sum_m f_m\eta_m=1\ , \tag{21}$$

where

$$\eta_m=\int d^3r\,F_m(\vec{r})\Big/\int_\Omega d^3r'\rho(\vec{r}')\ . \tag{22}$$

We can reduce the problem to one of matrix algebra if we introduce a nuclear lattice charge ρ_N to each electronic density, thereby giving the requisite cell-by-cell neutrality, to the interaction term in Eq. (15). Let us consider the identity

$$\begin{aligned}[\tilde{F}_m-\eta_m\rho_N \mid \rho-\rho_N]-\left[\tilde{F}_m-\eta_m\rho_n \left| \sum_n f_n(\tilde{F}_n-\eta_n\rho_N)\right.\right] \\ =\left[\tilde{F}_m \left| \rho-\sum_n f_n\tilde{F}_n \right.\right]-\left[1-\sum_n f_n\eta_n\right][\tilde{F}_m-\eta_m\rho_n \mid \rho_N]-\eta_m\left[\rho_N \left| \rho-\sum_n f_n\tilde{F}_n \right.\right]\ .\end{aligned} \tag{23}$$

The first term of the right-hand side of Eq. (23) is zero according to Eq. (20). Equation (21) plus the additional requirement that $[\tilde{F}_m-\eta_m\rho_N \mid \rho_N]$ be finite forces the second term of the right-hand side of Eq. (23) to zero. The term $[\rho_N \mid \rho-\sum_n f_n\tilde{F}_n]$ must also be finite (again by charge neutrality) for thin films; therefore Eq. (23) reduces to

$$\left[\sum_n f_n[\tilde{F}_m-\eta_m\rho_N \mid \tilde{F}_n-\eta_n\rho_N]-[\tilde{F}_m-\eta_m\rho_N \mid \rho-\rho_N] \right.\Big]=\eta_m\lambda\ , \tag{24}$$

where

$$\lambda=\left[\rho_N \left| f-\sum_n f_n\tilde{F}_n \right.\right] \tag{25}$$

is an undetermined constant independent of the index m in Eq. (25). Restating Eq. (24) in matrix notation yields

$$\sum_n B_{mn}f_n=a_m+\lambda\eta_m\ , \tag{26}$$

where

$$B_{mn}=[\tilde{F}_m-\eta_m\rho_N\,|\,\tilde{F}_n-\eta_n\rho_N]\,, \tag{27}$$

$$a_m=[\tilde{F}_m-\eta_m\rho_N\,|\,\rho-\rho_N]\,. \tag{28}$$

This set of equations is similar to the equations resulting from a least-squares-fitting procedure which includes a linear constraint equation. Thus we may solve for λ as

$$\lambda=\frac{\left[1-\sum_{mn}\eta_m\{B^{-1}\}_{mn}a_n\right]}{\left[\sum_{mn}\eta_m\{B^{-1}\}_{mn}\eta_n\right]}\,. \tag{29}$$

The solution for the coefficients f_m is then given by

$$f_m=\sum_n\{B^{-1}\}_{mn}(a_n+\lambda\eta_n)\,. \tag{30}$$

We see that the approximate electrostatic interaction energy defined in Eq. (17) now has the form

$$\tilde{U}=\sum_n f_n a_n-\tfrac{1}{2}\sum_{mn}f_m B_{mn}f_n \tag{31}$$

$$=[\tilde{\rho}\,|\,\rho]-\tfrac{1}{2}[\tilde{\rho}\,|\,\tilde{\rho}]-[\rho\,|\,\rho_N]+\tfrac{1}{2}[\rho_N\,|\,\rho_N]\,, \tag{32}$$

which is the electrostatic energy of the combined electronic and nuclear charges with only the electron repulsion term being replaced by an approximate interaction. These fitting procedures have been implemented computationally; some of the more pertinent details of the implementation are discussed in the context of the two applications to which we now turn.

III. RESULTS

The atomic hydrogen monolayer was chosen as the initial test case because atomic hydrogen contains only one electron and may be treated adequately with a small number of basis functions. Calculations have been performed on two lattice structures (square and hexagonal) with the value of α chosen as $\frac{2}{3}$ for simplicity. Preliminary calculations were reported in I which used a minimal basis set of three s-type Gaussian functions taken from van Duijneveldt.[11]

The values of the wave vector $\vec{k}$ were chosen in I such that all orbitals were periodic over a translation equal to four times that of any primitive lattice translation. Figure 2 illustrates the Brillouin zones and their irreducible regions for the square and hexagonal lattices. The 16 evenly spaced nonequivalent (by translation symmetry) wave vectors generated by the above-mentioned periodic boundary conditions are reduced by point-group symmetry to seven nonequivalent wave vectors for the square lattice and four wave vectors for the hexagonal lattice [see Figs. 2(b) and 2(e)]. The original calculation in I indicated that the square-lattice structure possessed a lower equilibrium cohesive energy per particle (-0.035 hartrees versus -0.005 hartrees) and thus a stable equilibrium geometry relative to the hexagonal structure.

More extensive calculations have been performed using a $(3s,1p)$ orbital basis set where p-type functions with exponents equal to 1.0 were added to the $3s$ basis as polarization functions. In addition to the slight improvement in the basis set, a finer wave-vector grid was used with the number of nonequivalent (by translation symmetry) points in the central Brillouin zone increased by 256. This choice increases the number of nonequivalent points [see Figs. 2(c) and 2(f)] in the Brillouin zone from 4 points to 30 points for the hexagonal lattice and from 6 points to 45 points for the square lattice.

The resulting cohesive energies per particle and virial ratios are presented as a function of the lattice constant for the square and hexagonal lattices in Tables I and II, respectively. A graphical display of the cohesive energies per particle is

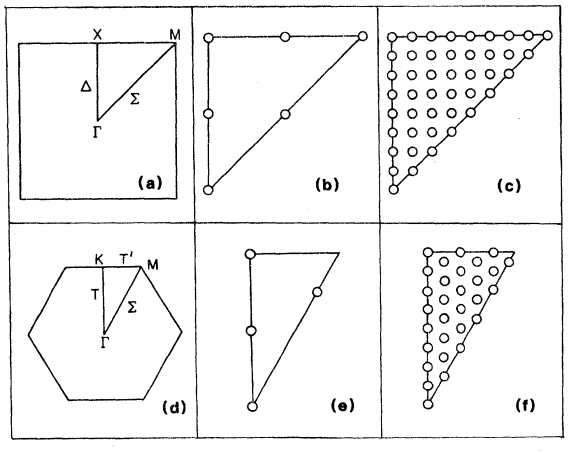

FIG. 2. (a) Central Brillouin zone for the square lattice and irreducible regions containing (b) six and (c) 45 evenly spaced points. (d) Central Brillouin zone for the hexagonal lattice with (e) four and (f) 30 evenly spaced points.

TABLE I. Calculated results for the square atomic hydrogen monolayer.

Lattice separation (a.u.)	Total energy (hartrees)	$-V/T$	Binding energy (hartrees)	(eV)
2.25	−0.4883	1.867	−0.0354	−0.963
2.50	−0.4921	1.995	−0.0391	−1.065
2.65	−0.4918	2.062	−0.0389	−1.057
2.75	−0.4909	2.103	−0.0380	−1.033
3.00	−0.4868	2.188	−0.0338	−0.920
5.00[a]	−0.4327	2.187	+0.0202	+0.550
5.00[b]	−0.4521	1.934	+0.0009	+0.024
100.00	−0.4530	1.972		

[a]Non-spin-polarized solution.
[b]Spin-polarized solution.

made in Fig. 3. The cohesive energies are calculated as the total energy minus the energy of the atomic monolayer at a lattice separation of 100 a.u. As can be easily seen, these results differ markedly from the results of I. Our earlier inference that the square lattice is the energetically preferred geometry at equilibrium is refuted by these more recent results. Most of the difference between the two sets of results appears attributable to the increase in the number of Brillouin-zone points, since the improvement in the basis from a $(3s)$ basis to a $(3s,1p)$ basis is quite modest compared to the increase of the total number of points in the Brillouin zone from 16 to 256.

It is to be noted that both Table I and Table II contain two sets of results for the lattice constant of 5.0 a.u. The use of the spin-polarized version of the computer code at this particular lattice separation (and only at this particular choice) leads to two stable (in the self-consistent iterative procedure) solutions that correspond to a non-spin-polarized (NSP) and completely spin-polarized (SP) solutions. Which result is obtained depends on the initial choice of fitting coefficients, since the use of coefficients corresponding to an SP system of overlapping atomic potentials yields the SP result, while starting with coefficients from the NSP state at 3.0 a.u. yields the NSP result. The NSP and SP results at a lattice constant of 5.0 a.u. evidently indicate that the bands corresponding to the different spins collapse at a lattice constant slightly less than 5.0 a.u. This conjecture was tested by calculating the cohesive energies per particle for both the NSP and SP modes at lattice constants equal to 6.0, 8.0, and 12.0 a.u. Figure 4 illustrates the results for these calculations and demonstrates the apparent crossing of the NSP state and the SP state at a lattice constant between 4.0 and 5.0 a.u. A similar phenomenon has been reported for the crystalline vanadium system[12] which exhibits the same collapse of bands of different spins to a doubly degenerate band as the lattice constant is decreased from the separated atom limit.

Beryllium is an interesting system to study using

TABLE II. Calculated results for the hexagonal atomic hydrogen monolayer.

Lattice separation (a.u.)	Total energy (hartrees)	$-V/T$	Binding energy (hartrees)	(eV)
2.25	−0.4823	1.784	−0.0293	−0.797
2.50	−0.4917	1.919	−0.0382	−1.040
2.65	−0.4924	1.990	−0.0394	−1.073
2.75	−0.4922	2.033	−0.0392	−1.066
3.00	−0.4892	2.131	−0.0363	−0.987
5.00[a]	−0.4378	2.229	+0.0151	+0.412
5.00[b]	−0.4503	1.923	+0.0027	+0.072
100.00	−0.4530	1.971		

[a]Non-spin-polarized solution.
[b]Spin-polarized solution.

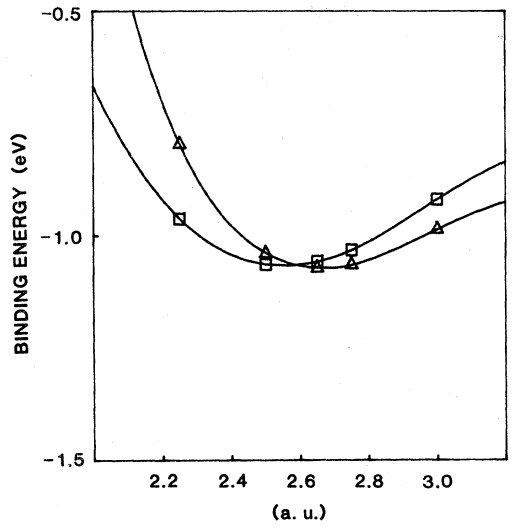

FIG. 3. Cohesive energy per particle vs lattice constant for square (□) and hexagonal (△) lattice structures of the atomic hydrogen monolayer.

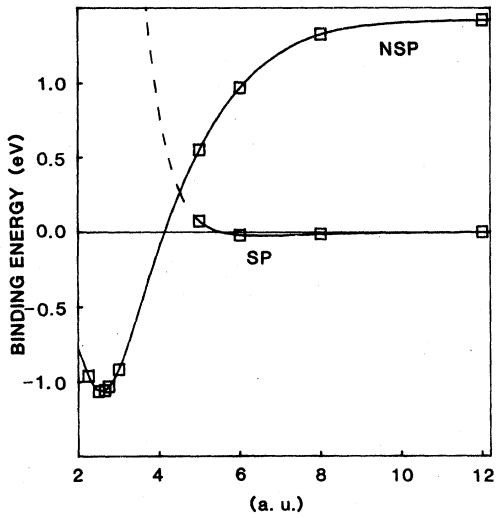

FIG. 4. Spin-polarized and non-spin-polarized cohesive energy per particle vs lattice constant for a square-lattice atomic hydrogen monolayer. Dashed portion of spin-polarized curve is extrapolated from the solid portion of the line.

the methods described in this work for several reasons. Recent experimental measurements of the work function of the (0001) surface of beryllium by Green and Bauer[13] indicate that beryllium has a work function of 5.1 eV, a value much higher than previous measurements had indicated. Until the results of Green and Bauer the recommended value of the work function according to the standard reference[14] was only 3.9 eV. Although Green and Bauer attribute this discrepancy in the work function to possible oxidation of the beryllium surface in the earlier work, these differences in experimental results pose a question worthy of theoretical investigation. The interpretation of certain peaks in the Auger spectra of beryllium[15] also poses questions appropriate for theoretical investigation using surface electronic structure computational methods.

In addition to the questions resulting from experimental study, beryllium is an interesting prototype system for studying the surface of metals. With only four electrons per atom, beryllium should require relatively modest amounts of computational effort for an adequate treatment of the surface. Beryllium is only weakly bound as a dimer, with a dissociation energy which is experimentally estimated to be about 0.7 eV.[16] The weak binding of the dimer is also indicated by theoretical calculations such as the configuration interaction calculations by Bender and Davidson,[17] which yield a strictly repulsive ground-state potential-energy curve, and the self-consistent-pair—coupled-electron-pair approximation (SCEP-CEPA) calculations by Dykstra, Schaefer, and Meyer[18] which lead to an estimate of the calculated dissociation energy as 0.03 eV at an equilibrium separation of about 8.5 bohr. Hartree-Fock calculations by Bauschlicher, Liskow, Bender, and Schaefer[19] and by Jordan and Simons[20] indicate the smallest cluster that exhibits appreciable binding (0.46 eV per atom) contains four beryllium atoms. This indicates that the cohesive energy of the solid (and presumably the monolayer as well) is probably due in large measure to the delocalization and indeed its extent can be assessed by comparing results for the infinitely extended monolayer obtained from the methods described in this work with the binding energies calculated by Bauschlicher[21] on beryllium clusters and with experimental results for the real surface.

We have performed calculations on the atomic beryllium monolayer using the $(6s,2p)$ basis given in Table III. The six s-type functions are taken from van Diujneveldt's[11] $6s$ basis for beryllium. The two p-type functions are the same as used by Bauschlicher[21] in his cluster calculations. Preliminary calculations on the dimer were performed with this basis using the molecular LCAO-$X\alpha$ program[7] and a plot of the binding energy versus the nuclear separation is presented in Fig. 5. These results are consistent with the previously mentioned results of Dykstra, Schaefer, and Meyer, and

TABLE III. Basis sets for the beryllium monolayer.

Orbital basis		Charge fitting basis		Exchange fitting basis	
Type	Exponent	Type	Exponent	Type	Exponent
s	0.067 376	s	0.134 752	s	0.044 917 3
s	0.198 210	s	0.396 420	s	0.132 140
s	1.767 558	s	3.535 116	s	1.178 372
s	6.819 528	s	13.639 056	s	4.546 352
s	30.827 597	s	61.655 194	s	20.551 731
s	204.906 144	s	409.812 29	s	136.604 096
x	0.509	s	1.018	s	0.339 33
x	0.118	s	0.236	s	0.079 667
y	0.509	x^2+y^2	1.018	x^2+y^2	0.339 33
y	0.118	x^2+y^2	0.236	x^2+y^2	0.079 667
z	0.509	z^2	1.018	z^2	0.339 33
z	0.118	z^2	0.236	z^2	0.079 667

demonstrate the weak binding of the beryllium dimer as well as provide a check on the balance of the $(6s,2p)$ basis set.

Since beryllium possesses a hexagonal close-packed structure in the solid, the calculations were performed on a hexagonal lattice of beryllium atoms. This structure is equivalent to a single layer from the (0001) surface of the crystalline solid. The beryllium lattice has the same Brillouin-zone symmetry as that of the hexagonal atomic hydrogen monolayer [Fig. 2(d)]. We used the same array of 30 nonequivalent points in the Brillouin zone for the beryllium as for the hexagonal atomic hydrogen monolayer calculations.

Table IV presents some results of our calculations giving the cohesive energies and virial ratios

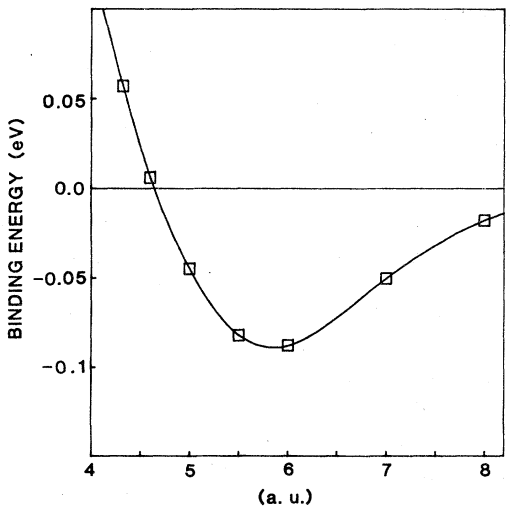

FIG. 5. Binding energy vs internuclear separation for beryllium dimer.

of the beryllium monolayer as a function of the lattice spacing. These results and Fig. 6 imply that the beryllium monolayer has an equilibrium lattice separation of 4.1 bohr and an equilibrium cohesive energy of -2.64 eV per particle. Since the virial theorem is valid for the $X\alpha$ method,[22] the virial ratio $-V/T$ should equal 2 at the minimum of the cohesive energy curve where the derivative of the cohesive energy with respect to the lattice spacing equals zero. We see in Table IV that the location of the cohesive energy minimum (predicted by interpolation of the virial ratios to yield a predicted lattice constant of 4.05 a.u. and an estimated cohesive energy per particle at that lattice constant of -2.63 eV) is in close agreement with that of the actual cohesive curve. These equilibrium results differ slightly from the bulk equilibrium separation of 4.321 bohr and equilibrium cohesive energy of -3.32 eV per particle,[23] but not more than could be attributed plausibly to the differences between monolayer and bulk solid beryllium.

Baushclicher[21] has performed calculations using the Hartree-Fock method on various size beryllium clusters with the same internuclear separation as the bulk solid. For the various monolayer clusters, he reports binding energies of $+0.22$ eV per particle for a three atom cluster, $+0.07$ eV per particle for a six-atom cluster, -0.16 eV per particle for a seven-atom cluster, and -0.63 eV per particle for a 14-atom cluster. The largest cluster he considered was a 22-atom cluster in two layers which yielded a computed binding energy of -0.89 eV per particle. These cluster results apparently indicate a trend in binding energies as the cluster size increases which should be consistent with our equilibrium cohesive energy of -2.64 eV per parti-

TABLE IV. Calculated results for the atomic beryllium monolayer.

Lattice separation (a.u.)	Total energy (hartrees)	$-V/T$	Binding energy (hartrees)	(eV)
3.80	−14.293 628	1.993 70	−0.092 185	−2.5084
3.90	−14.296 508	1.995 53	−0.095 065	−2.5867
4.00	−14.298 019	1.998 80	−0.096 576	−2.6278
4.10	−14.298 351	2.001 49	−0.096 908	−2.6369
4.25	−14.297 454	2.005 86	−0.096 011	−2.6125
4.321	−14.296 885	2.005 66	−0.095 442	−2.5970
4.50	−14.293 275	2.008 37	−0.091 832	−2.4987
5.00	−14.275 816	2.014 93	−0.074 373	−2.0237
6.00	−14.234 844	2.012 63	−0.033 401	−0.9088
100.00	−14.201 443	1.999 01		

cle, although one may infer that much larger clusters are necessary for a proper treatment of the cohesive energy of the beryllium monolayer. This is a point in favor of our earlier contention that a primary cause of the binding energy of the beryllium monolayer is the delocalization of the electronic charge over many nuclear sites.

Band energies were interpolated for 4096 points in the Brillouin zone using a scheme adapted from the method proposed by Monkhorst and Pack[24] for three-dimensional Brillouin-zone interpolations. This method uses a discrete Fourier transform over the 256 evenly spaced points in the complete Brillouin zone for which the band energies are computed. Band energies at intermediate points were then evaluated using the resulting Fourier expansion. Figure 7(a) displays the valence bands and lower empty bands computed for the beryllium monolayer at the equilibrium lattice spacing of 4.10 a.u. The shape of the bands resembles qualitatively the bands reported by Loucks and Cutler[25] for crystalline beryllium, if we compare our results with the solid energy bands for wave vectors lying in planes parallel to the plane of the periodicity of the monolayer. One reasonably may assume that the discrepancy between our bands and those of Loucks and Cutler is due to the differences between the monolayer and the crystal, and that the addition of more layers would lead to multilayer bands more in agreement with those of the crystalline beryllium solid. Further work is underway on calculations involving more than one layer of beryllium.

We estimate the work function of beryllium from the negative of the Fermi energy of our calculations.[23] We find that our Fermi energy for the

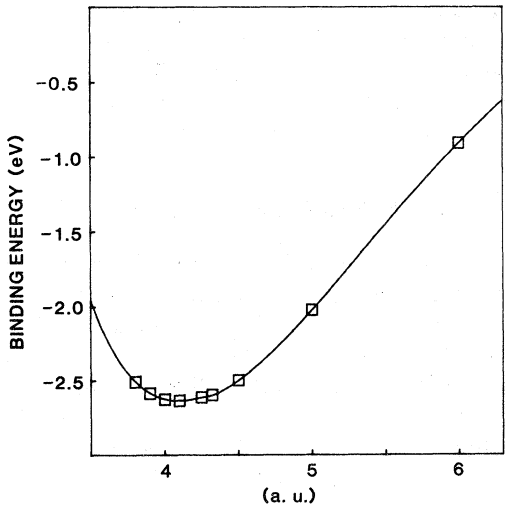

FIG. 6. Cohesive energy per particle vs lattice constant for the hexagonal beryllium monolayer.

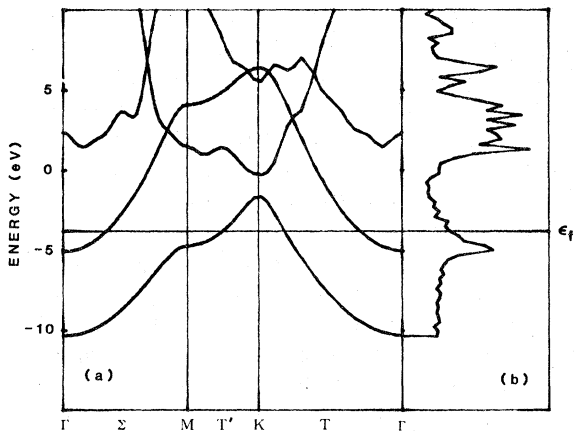

FIG. 7. (a) Valence-band structure and (b) total density of states for the hexagonal atomic beryllium monolayer.

monolayer of -3.80 eV agrees quite well with the recommended value of Fomenko.[14] However, the study by Trickey *et al.*[26] indicates that while the choice of α equal to $\frac{2}{3}$ will yield reasonable cohesive energies and bandwidths, one expects that this value of α will lead to underestimating band gaps and the Fermi energy. Thus the fact that we anticipate our Fermi energy to underestimate the work function, and that increasing the number of layers will probably change the Fermi energy in a manner not easily predictable, our estimated work function of 3.80 eV is not necessarily in conflict with the reported experimental work function of 5.10 eV.[13]

The density of states for the beryllium monolayer is presented in Fig. 7(b). The results are also consistent and in qualitative agreement with the density of states computed for the crystalline beryllium solid.[25] The relatively flat region in the density of states at energies around -10.0 eV in Fig. 7(b) is understandable when one notices that the bands in Fig. 7(a) are nearly-free-electron-like in character. One can demonstrate that the density of states for a two-dimensional electron gas will be a step function. Thus the flat region of our density of states is due to the nearly-free-electron-like behavior of the bottom of the lowest band in Fig. 7(a).

Musket and Fortner[27] have reported auger electron spectroscopy (AES) results for beryllium indicating two peaks at 92 and 104 eV. Later work by Suleman and Pattinson[15] indicates that the AES peak at 93 eV was evidently due to impurities on the beryllium surface, although they agreed with the earlier conclusion of Musket and Fortner that the peak at 104 eV was due to a $(2p,2p)$ KVV transition at the solid surface. The energy of this transition will equal the energy difference of an electron in the $2p$ band (ϵ_{2p}) and the energy of the hole it fills in the core K shell (ϵ_K) minus the energy required to excite an electron from some different location in the $2p$ band (ϵ'_{2p}). We may thus find an estimate for the peak of the above mentioned transition by taking the difference $\Delta\epsilon=\epsilon_{2p}+\epsilon'_{2p}-\epsilon_K$. To find appropriate bounds for our estimate (since we do not anticipate monolayer results more accurate than 2 or 3 eV in light of our previous discussion of the effects of adding more layers to the beryllium system) we may consider ϵ_{2p} and ϵ'_{2p} jointly equal either to the bottom of the second band in Fig. 7(a), which corresponds to the $2p_z$ band, or to the Fermi energy. Since we anticipate that the band energy for the core band will not be very accurate, we will use the reported results of -111 eV plus the work function.[28] Depending upon whether we use the experimental work function or our estimated work function, we find a range of 105 to 109 eV for our estimate of the $(2p,2p)$ KVV Auger peak. Thus we find one more source of agreement of our monolayer results with those of the bulk solid, indicating that even these simple monolayer calculations provide useful information for describing the surface of the bulk solid.

IV. SUMMARY

The chief objective of this work has been to demonstrate the usefulness of a new combination of computational techniques for studying the electronic structure of thin-layer systems. The physically reasonable results produced for the hydrogen monolayer indicate that there are no inherent flaws in the mathematical formalism. The beryllium monolayer results further indicate the feasibility of our approach as well as demonstrating the applicability to experimentally interesting systems. The comparison of our theoretically estimated values for the equilibrium lattice spacing, equilibrium cohesive energy per particle, and work function with the experimentally determined quantities for the beryllium system and with other calculated results indicates that even such a simple model as the monolayer yields useful results. The primary difficulty with this approach as of now has been the amount of computer time required to produce adequately precise results for systems larger than the atomic beryllium monolayer. Steps are currently being taken to develop new algorithms for the computer code to reduce this difficulty.

ACKNOWLEDGMENTS

J.W.M. thanks B. I. Dunlap for his helpful advice and discussions on this work. Grants of computer time from the Northest Regional Data Center of the State University System of Florida and from the Department of Highway Safety and Motor Vehicles of the State of Florida are both gratefully acknowledged. This work was supported in part by NSF Grant No. DMR 79-09721.

*Based in part on the Ph.D. dissertation of J. W. M., University of Florida.
†Present address: Code 6171, Naval Research Laboratory, Washington, D. C. 20375.

[1]J. G. Gay, J. R. Smith, and F. J. Arlinghaus, Phys. Rev. Lett. 38, 561 (1977); Phys. Rev. B 21, 2201 (1980); 21, 2055 (1980).
[2]C. S. Wang and A. J. Freeman, Phys. Rev. B 18, 714 (1978); 19, 793 (1979); 21, 4585 (1980).
[3]J. A. Appelbaum and D. R. Hamann, Solid State Commun. 27, 881 (1978); P. J. Feibelman, J. A. Appelbaum, and D. R. Hamann, Phys. Rev. B 20, 1433 (1979); P. J. Feibelman and D. R. Hamann, *ibid.* 21, 1385 (1980); P. J. Feibelman and F. J. Himpel, *ibid.* 21, 1394 (1980).
[4]J. W. Mintmire and J. R. Sabin, Inter. J. Quantum Chem. S14, 707 (1980).
[5](a) J. W. D. Connolly, in *Modern Theoretical Chemistry,* edited by G. A. Segal (Plenum, New York, 1976), Vol. 7, and references therein; (b) Also see U. von Barth and L. Hedin, J. Phys. C 5, 1629 (1972).
[6]B. I. Dunlap, J. W. D. Connolly, and J. R. Sabin, J. Chem. Phys. 71, 3396 (1979).
[7]J. W. Mintmire, Int. J. Quantum Chem. S13, 163 (1979).
[8]H. Sambe and R. Felton, J. Chem. Phys. 62, 1122 (1975).
[9]B. I. Dunlap, J. W. D. Connolly, and J. R. Sabin, Int. J. Quantum Chem. S11, 81 (1977).
[10]J. W. Mintmire, Ph.D. dissertation, University of Florida (1980) (unpublished).
[11]F. B. van Duijneveldt, IBM Report No. RJ945 (unpublished).
[12]T. M. Hattox, J. B. Conklin, J. C. Slater, and S. B. Trickey, J. Phys. Chem. Solids 34, 1627 (1973).
[13]A. K. Green and E. Bauer, Surf. Sci. 74:, 676 (1978).
[14]V. S. Fomenko, *Handbook of Thermionic Properties* (Plenum, New York, 1966).
[15]M. Suleman and E. B. Pattinson, J. Phys. F 1, L24 (1971).
[16]A. G. Gaydon, *Dissociation Energies and Spectra of Diatomic Molecules* (Chapman and Hall, London, 1968).
[17]C. F. Bender and E. R. Davidson, J. Chem. Phys. 47, 4972 (1967).
[18]C. E. Dykstra, H. F. Schaefer, and W. Meyer, J. Chem. Phys. 65, 5141 (1977).
[19]C. W. Bauschlicher, D. H. Liskow, C. F. Bender, and H. F. Schaefer, J. Chem. Phys. 62, 4815 (1975).
[20]K. D. Jordan and J. Simons, J. Chem. Phys. 67, 4027 (1977).
[21]C. W. Bauschlicher, Ph.D. dissertation, 1976 (unpublished).
[22]J. C. Slater, J. Chem. Phys. 57, 2389 (1972).
[23]C. Kittel, *Introduction to Solid State Physics,* 5th edition (Wiley, New York, 1976).
[24]H. J. Monkhorst and J. D. Pack, Phys. Rev. B 13, 5188 (1976).
[25]T. L. Loucks and P. H. Cutler, Phys. Rev. 133, A819 (1964).
[26]S. B. Trickey, A. K. Ray, and J. P. Worth, Phys. Status Solidi B 106, 613 (1981).
[27]R. G. Musket and R. J. Fortner, Phys. Rev. Lett. 26, 80 (1971).
[28]K. Siegbahn, C. Nordling, A. Fahlman, R. Nordberg, K. Hamrin, J. Hedman, G. Johansson, T. Bergmark, S. E. Karlsson, I. Lindgren, and B. Lindberg, *ESCA: Atomic, Molecular, and Solid State Structure Studied by Means of Electron Spectroscopy* (Almqvist and Wiksells, Uppsala, 1967).